C029

Sub-basalt Imaging Using Broadside CSEM

J.P. Morten* (EMGS), S. Fanavoll (EMGS), F.M. Mrope (EMGS) & A.K. Nguyen (EMGS)

SUMMARY

Marine controlled source electromagnetic measurements in the broadside source-receiver configuration enables mapping of base basalt and underlying structure. We study a case where the spatial resolution of magnetotelluric data is too low to map a thin basaltic layer, making CSEM an important exploration tool that can provide structural information to identify prospects and aid seismic processing. Improvements in acquisition and processing technology are shown to further extend the application window demonstrated in previous studies.

Introduction

Sub-basalt plays are receiving increasing interest in the exploration for oil and gas. Besides basalt acting as a direct seal for hydrocarbon accumulations, there are a variety of traps that can be hidden below a basalt layer. However, due to shape irregularities and heterogeneities with high velocity contrasts around and within the basalts, it can be challenging for seismic processing to image the base of the basaltic layer and details of what is below. [For example, see Fliedner and White (2001)]. Hence, methods that improve mapping of basalt and the sediments below will be of great value for the petroleum industry.

It has been demonstrated previously by MacGregor and Sinha (2000) that the marine controlled source electromagnetic (CSEM) method can provide large-scale, low resolution structural information of basalt and underlying layers, in particular in conjunction with marine magnetotellurics (MMT), MacGregor (2003). These studies focussed on thick basalt layers at the kilometre scale and thicker.

In this paper, we will focus on thinner basalt layers. We assume that MMT data is only available at low frequencies, such that only the structure at the largest scale can be resolved with these data. This makes CSEM data acquired in the broadside configuration an essential and unique component in the imaging. The inline CSEM data is sensitive to the top of the basaltic layer with reduced penetration, but the broadside data gives the desired sensitivity to deeper structure and base of basalt. Our study also takes into account recent improvements in acquisition and processing which have significantly raised the effectiveness of this technique in addressing the basalt problem. The improvements include among others: 1) Improved receivers with noise level lower than 0.1 nV/m (assuming deep water and 100 periods of stacking) and precise timing (< 1 millisecond drift in 14 days). 2) Acquisition vessels capable of managing up to 200 receivers enabling larger data fold. 3) Stronger source (> 300 000 Am). 4) 3D anisotropic inversion as well as improved calibration and pre-processing tools. These improvements are here shown to give resolution down to ~100 m.

CSEM responses

The CSEM source is a horizontal dipole towed close to the seafloor. Inline data is measured at receivers lying along the trajectory of the towed source. Broadside data is measured at receivers on a line perpendicular to the dipole source. State-of-the-art 3D surveys have receivers on a grid and multiple tow lines, often with a range of tow line directions. This yields a rich dataset with both inline and broadside data, but require substantial vessel time to acquire. A 2D CSEM survey for early exploration stage mapping can be acquired faster, but typically deliver very limited broadside data. We study regional mapping with a 90 km long 2D CSEM line, which gives broadside data, but requires dense deployment of receivers 500 m apart. A single tow along the receiver line provides inline data, and additional, short cross-lines placed with 3 km intervals provide broadside data. The short receiver spacing assumed provides broadside data at a denser offset sampling, and reflects current capacity of modern vessels. Future developments may facilitate towing of a cross-dipole source, which gives both inline and broadside data with larger receiver spacing without cross-lines.

Let us first consider the differences in sensitivity for thick resistive structures between inline and broadside CSEM data. Inline measurements are very sensitive to the presence of resistive layers, since the electrical field in that case couples to the resistor with a large vertical component. This reflects a series coupling of the resistor with the conductive environment, and results in a partially guided wave event. Since the guided wave pertains also for thin resistors due to the effective series coupling, inline CSEM measurement are successfully utilized in exploration for hydrocarbons which constitute thin resistive anomalies (Constable and Srnka, 2007). However, the guiding effect reduces the sensitivity to structures below the resistor, due to the dominant guiding contribution. CSEM data from a broadside configuration, on the other hand, couple with a large horizontal electrical field and is sensitive to the resistivity resulting from a parallel coupling of layers. The broadside data, similar to MMT data, thus has limited sensitivity to thin resistors. The reduced guiding effect for broadside measurements does however imply a relatively larger sensitivity to conductive structures below.

To study the sensitivity of inline and broadside data to structure below a resistor, we consider the synthetic model shown in Figure 1. The ultra-deep water model (0.27 Ωm) has an overburden (3 Ωm) over a wedge shaped basalt layer (100 Ωm). Below the basalt there is a sedimentary layer (2 Ωm) and a non-crystalline basement (10 Ωm). The structures are invariant in the direction perpendicular to the figure. The shape of the basalt layer allows us to study the sensitivity to structures below as a function of the thickness. We expect that the sensitivity decays with increasing basalt thickness. For simplicity, we have here assumed homogeneous basalt. However as shown by MacGregor (2003), the CSEM response to a stack of thin alternating resistors is very similar to a thick homogeneous resistor with an average resistivity.
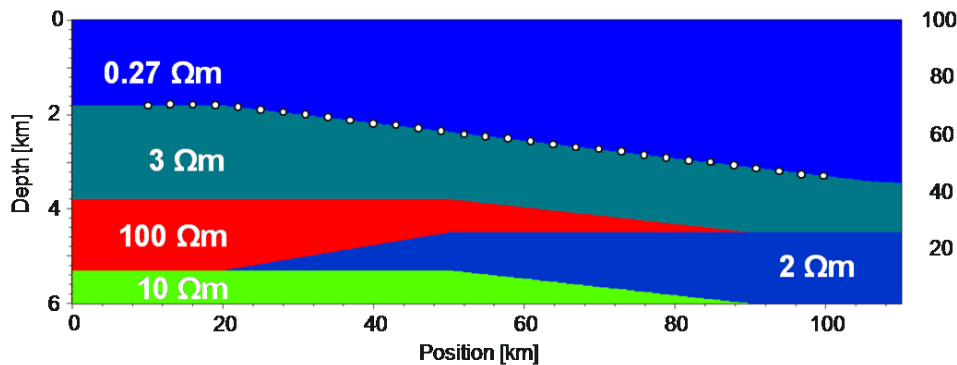

Figure 1 *True model. Layers (top to bottom): Seawater, overburden, basalt, sediments, and basement.*

In order to analyze the sensitivity of the CSEM data, we compare data from the true model to a basalt flooded model where the sediment and the basement resistivities are replaced by 100 Ωm. This model represents the information available after a seismic survey which was only able to image the top basalt. Simulated electric field data from a current dipole source was created for the 31 receiver sites indicated in Figure 1, with receiver separation 3 km. Source positions were created each 500 m along the receiver line, with the source having two polarizations, inline and broadside. In a real acquisition, such dataset should be acquired by interchanging source and receiver positions using reciprocity. Figure 2 shows the normalized data difference between true model and basalt-flooded model, $|E_{True}-E_{Flood}|/|E_{True}|$, common mid-point (CMP) sorted. A response at e.g. 1 in these plots means that the difference between data from the true and basalt flooded models is 100 % of the data magnitude.
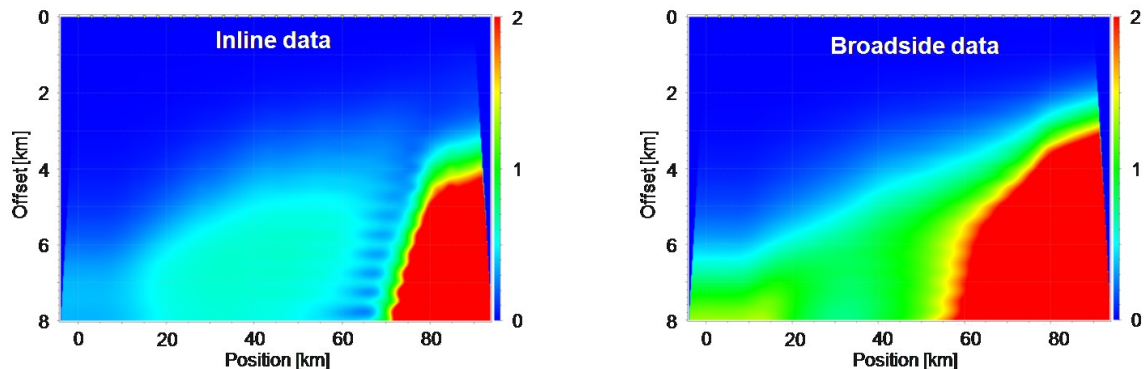

Figure 2 *CMP sorted normalized data difference at 1.5 Hz between true model and basalt flooded model (interpolated between data points). Left plot shows inline data, right plot broadside data.*

Consider first the plot of inline normalized data difference. The rightmost part of the model shows the strongest response because in this region the resistive layer is completely pinched out in the true model. Moving towards the left in the figure, we see that the data difference quickly decays due to increasing resistor thickness and associated reduced sensitivity. Below the thickest (1.5 km) part of the resistor, the response falls to 35 % and the signal level approaches the noise level 0.1 nV/m. The data therefore has significant information about structures below the basalt also in this region, but since it is marginal, reliable imaging is questionable.

The broadside normalized data difference shows that the response is largest from the area where the resistive layer is pinched out, similar to the inline data. Moving left towards the part with thicker basalt, we see a qualitatively different behaviour than inline data. The normalized response does not decay much with increasing resistor thickness, only a shift towards larger offset is observed. For the whole thickness interval probed by this model, the broadside data response remains large at more than 100 % with a signal magnitude above the noise level even at the farthest offset plotted.

In summary, the broadside data responses provide information about structures below the basalt three times more significant than inline data. It has a qualitatively different dependence on the basalt thickness. The response of inline data decays rapidly with resistor thickness, whereas broadside data responses remain large for the thicknesses studied here. We can therefore expect that imaging of sub-basalt structures that can utilize broadside data will yield more accurate descriptions and be more robust than imaging based on inline data alone.

CSEM inversion results

Figure 3 shows the 3D inversion result for the synthetic data based on the true model. The 3D inversion tool is described in Zach et al. (2008). To speed up the convergence, the initial model is created by 31 independent 1D inversions, one for each CMP sorted gather. Top basalt is assumed known, such that the overburden is treated as a single layer in the 1D inversions. No other regularization or constraint is employed at any stage of the inversions. We inverted the broadside and inline data at frequencies 0.6, 1.0, and 1.5 Hz. Figure 3 shows that base basalt is imaged to about 100 m accuracy when the thickness is lower than 1 km. In this region the sediments and the basement are also imaged adequately, both in terms of structure and resistivity. As the basalt thickens, imaging of the structures below becomes poorer, but the result still identifies base basalt to about 300 m accuracy. The data misfit was generally below 10 % relative to the true model data amplitude, but shows some significant residuals at far offset for the central receivers indicating that more information could still be extracted from the data.

In addition to the result shown in Figure 3, we also inverted broadside and inline data separately, as well as different frequency combinations (not shown). Inline data only inversion gives much poorer results than the broadside data only inversion, which is expected due to the difference in sensitivity discussed above. In particular, the base basalt was not imaged using only inline data when the thickness exceeded 1 km.
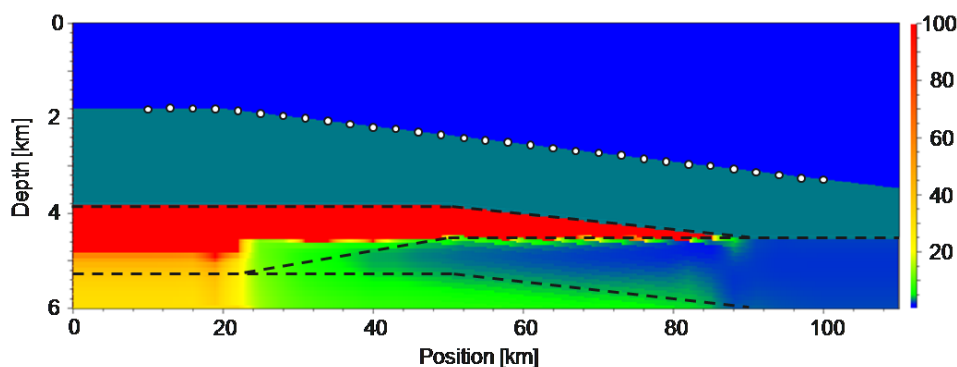

Figure 3 *Final resistivity model (Ωm) from 3D inversion of broadside and inline electrical field data at 0.6, 1.0, and 1.5 Hz. White dots show 3 km spaced cross-lines, dashed lines show true model layers.*

Marine magnetotelluric (MMT) inversion

As discussed in the introduction, MMT data has been applied to image structures below thick resistive layers. [For a recent example see Virgilio *et al*. (2010)]. The scenario discussed in this paper, with ultra-deep water and a pinching out basalt layer may be challenging for MMT applications. The water column will attenuate the higher frequency part of the MMT spectrum, which we expect to be

essential for proper imaging of the thinner parts of the resistive layer. In order to study this prediction, we have performed 2D MMT inversion using the same 3 km sampling as in the CSEM case and with data at 20 frequencies from 1/20 to 1/1500 Hz, a typical range observed in proprietary datasets in deep water and at low latitude. The initial model was the same flooded model used for the CSEM inversion to make a fair comparison. The final model central section is shown in Figure 4. The MMT inversion result lacks resolution to identify the basalt and sediment layers, but provides a reasonably good image of the basement. The data fit for this result was on the scale of the expected survey accuracy.
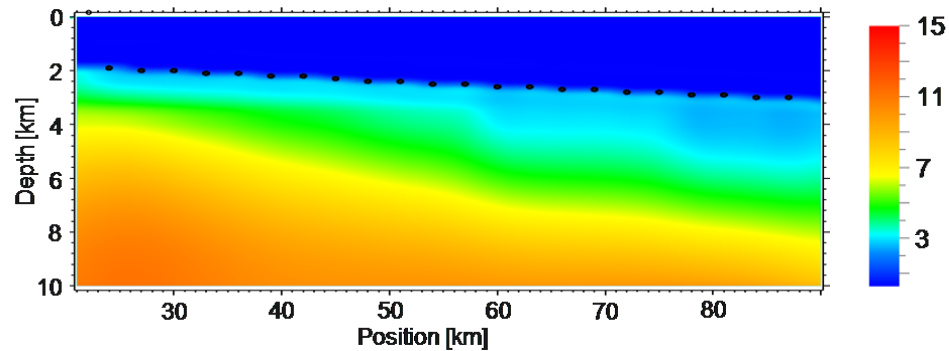

Figure 4 *Final resistivity model (Ωm) from MMT inversion.*

Conclusions

We have studied synthetic CSEM data from a model with a variable thickness basalt layer overlaying conductive structures. We demonstrated that the improved data quality and processing algorithms can enhance the sub-basalt imaging resolution to ~100 m. The results also apply for sub-salt or sub-carbonate structures. The broadside configuration measurements show large sensitivity to the conductive structures even when the basalt layer is as thick as 1.5 km, and inversion of the data demonstrates how CSEM can be utilized to map base basalt and even image the sediments and basement below. At the same time we show that MMT data in a deep water environment provides inadequate resolution to reliably indentify the structures. In this case the broadside CSEM data provides exclusive information to assess possible reservoir presence in environments where basalt layers cover conductive reservoir rock. Information about base basalt will also provide better velocity models that improve seismic processing and imaging. Looking ahead, we have studied the response of a 100 m thick, 6 km diameter, disc shaped resistor (100 Ωm) underneath the basalt, representing a hydrocarbon reservoir. Below 500 m of basalt, this inclusion gives only 12 % response, so reliable imaging of this feature will be challenging at the present stage.

References

Constable, S. and Srnka, L.J. [2007] An introduction to marine controlled-source electromagnetic methods for hydrocarbon exploration. *Geophysics,* **72**, WA3-WA12 (2007).

Fliedner, M.M. and White, R.S. [2001] Seismic structure of basalt flows from surface seismic data, borehole measurements and synthetic seismogram modelling. *Geophysics* **66**, 1925 (2001).

MacGregor, L., and Sinha, M. [2000] Use of marine controlled-source electromagnetic sounding for sub-basalt exploration. *Geophysical prospecting* **48**, 1091 (2000).

MacGregor, L. [2003] Joint analysis of marine active and passive source EM data for sub-salt or sub-basalt imaging. *65th EAGE Conference & Exhibition, Expanded abstract* **F18** (2003).

Virgilio, M., De Stefano, M., Re, S., Golfè Andreasi, F., and Snyder, F.F.C. [2010] Simultaneous Joint Inversion of Seismic, Gravity, and EM Data for Subsalt Depth Imaging in Gulf of Mexico. *72nd EAGE Conference & Exhibition, Expanded abstract* **K045** (2010).

Zach, J. J., Bjørke, A. K., Støren, T., and Maaø, F. [2008] 3D inversion of marine CSEM data using a fast finite-difference time-domain forward code and approximate hessian-based optimization. *SEG Expanded Abstracts* **27**, 614 (2008).